

# Towards Matrix-Free Patch Smoothers for the Stokes Problem: Evaluating Local $p$ -Multigrid Solvers

Michał Wichrowski<sup>0</sup>

## Abstract

Vertex-patch smoothers offer an effective strategy for achieving robust geometric multigrid convergence for the Stokes equations, particularly in the context of high-order finite elements. However, their practical efficiency is often limited by the computational cost of solving the local saddle-point problems, especially when explicit matrix factorizations are not feasible. We explore a fully iterative, matrix-free-compatible approach to the local patch solve using  $p$ -multigrid techniques. We evaluate different local solver configurations: Braess-Sarazin and block-triangular preconditioners. Our numerical experiments suggest that the Braess-Sarazin approach is particularly resilient. We find that a single iteration of the local solver yields global convergence rates comparable to those obtained with exact local solvers, even on distorted meshes and in the presence of large viscosity jumps.

**Keywords:** finite element method, multigrid method, vertex-patch smoothing, Stokes equations, matrix-free

**AMS subject classifications:** 65Y10, 65Y20, 65N55, 65N30

## 1 Introduction

Geometric multigrid methods establish the gold standard for elliptic partial differential equations, delivering optimal  $\mathcal{O}(N)$  complexity for symmetric positive definite problems [16, 7, 38]. However, extending this efficiency to the Stokes equations presents a fundamental structural challenge: the smoother must not only reduce high-frequency errors in the velocity but also effectively damp error components within the divergence-free subspace. Standard point-wise or cell-wise smoothers often fail in this regard because the support of discrete divergence-free basis functions typically extends beyond a single element, preventing the local resolution of the mass conservation constraint. Vertex-patch smoothers overcome this by solving coupled problems on overlapping subdomains that fully enclose these supports, thereby recovering the stability of the splitting [18, 21]. The potential efficiency of this approach is close to direct solving the system; for instance, recent work on GPU-accelerated solvers utilizing Raviart-Thomas elements [36, 32] demonstrated global convergence in as few as 2 to 3 iterations [13]. Yet, realizing this efficiency for general high-order discretizations requires overcoming the significant computational bottleneck of solving these local patch problems.

While high-order methods offer superior approximation properties and favorable dispersion error characteristics [14], they induce linear systems that are expensive to solve using traditional matrix-based approaches. The memory bandwidth bottleneck associated with assembling and storing large, dense element matrices has driven a paradigm shift toward matrix-free implementations [22, 23]. By leveraging sum-factorization techniques on tensor-product cells, matrix-free methods reduce

---

<sup>0</sup>Interdisciplinary Center for Scientific Computing, Heidelberg University, Germany. [mt.wichrowsk@uw.edu.pl](mailto:mt.wichrowsk@uw.edu.pl)

the operator evaluation cost to  $\mathcal{O}(p^{d+1})$  and minimize data movement, which is critical on modern hardware architectures [24, 31]. However, this matrix-free constraint severely limits the choice of available preconditioners and smoothers, as access to individual matrix entries is no longer possible.

To address the need for robust smoothing in high-order, matrix-free regimes, overlapping domain decomposition techniques: specifically vertex-patch (or vertex-star) smoothers, have emerged as a powerful solution. Originally analyzed in the context of domain decomposition [34, 3], these methods decompose the global domain into small, overlapping subdomains centered around mesh vertices. By solving local problems on these patches, they capture the local high-frequency spectrum of the operator, providing robust smoothing that is independent of the mesh size  $h$  and often the polynomial degree  $p$  [19, 21]. This approach has recently gained traction for complex problems, including non-matching grid methods [41, 12, 4] and  $H(\text{div})$ -conforming discretizations [18]. Moreover, the patch-based structure naturally promotes excellent data locality with high arithmetic intensity, making it highly suitable for parallelization on both CPUs [46, 43] and GPUs [11].

Despite these advantages, the adoption of patch smoothers is traditionally hindered by a single, critical bottleneck: the computational cost of solving the local patch problems. For scalar elliptic problems, such as the Poisson equation, highly efficient local solvers have been developed. These range from fast diagonalization methods (FDM) exploiting tensor-product separability on structured grids [47, 48] to specialized direct solvers that utilize static condensation and Cholesky factorization [8]. However, for the Stokes equations, there is no such *silver bullet*. The coupling between velocity and pressure, combined with the Schur complement, breaks the operator's separability even on perfectly Cartesian grids. Consequently, fast diagonalization cannot be directly applied to the full system.

The literature offers several strategies to tackle the global Stokes system, which influence the design of local solvers. A prominent class is block preconditioning [25, 26], where the system is decoupled into velocity and pressure sub-problems. These methods typically employ approximations of the pressure Schur complement, such as the pressure mass matrix or diffusion operators [33]. While effective as global preconditioners, their application within a local patch smoother has not been studied. The local patch problems inherit the indefinite nature of the global system, and constructing robust block preconditioners that respect the local boundary conditions of the patch – especially on distorted meshes – remains an open challenge.

An alternative approach, specifically designed for multigrid smoothing, is the class of coupled *Vanka* or box-relaxation smoothers [39]. These methods solve small, local saddle-point systems associated with a cell or a cluster of degrees of freedom. *Vanka* smoothers have been extensively studied and applied to various discretizations [49, 15], including variable viscosity problems [5] and space-time formulations [28, 29]. While classical *Vanka* smoothers often rely on dense local inverses or direct solvers, recent efforts have explored inexact or compressed variants to reduce computational load [17]. However, ensuring the  $p$ -robustness of these coupled smoothers without incurring excessive cost remains a difficulty, particularly for matrix-free high-order methods where forming the local dense matrix comes at a prohibitive cost.

The robustness of the local solver becomes paramount when targeting complex physical applications characterized by large jumps in material coefficients. Two prime examples are Geodynamics, specifically mantle convection [37, 9], and Fluid-Structure Interaction (FSI) [45, 40]. In FSI problems solved via monolithic schemes, the solid subdomain behaves as a fluid with extremely high viscosity (pseudo-viscosity proportional to the inverse time step), leading to viscosity contrasts of orders  $10^6$  to  $10^{12}$  across the interface. Similarly, mantle convection involves viscosity variations of several orders of magnitude due to temperature and pressure dependence. In such regimes, standard smoothers often stall. The local patch solver must therefore be robust not only to mesh distortion but also to extreme coefficient heterogeneity, effectively capturing the local interface

dynamics [33, 30].

A promising candidate for handling these difficult regimes is the Braess-Sarazin smoother [6]. As elegantly described in [10], this method can be interpreted as a constrained smoother that effectively handles the saddle-point structure by maintaining the velocity-pressure coupling. While it has not been the standard choice in the broader community, recent investigations have demonstrated its specific efficacy for matrix-free implementations [44, 20]. Furthermore, it has been shown to perform reasonably well for the extreme viscosity contrasts inherent in Fluid-Structure Interaction problems [45]. However, utilizing Braess-Sarazin as a *local* solver inside a vertex-patch smoother implies a nested complexity: one must solve a saddle-point problem inside a patch, which itself is part of a global multigrid hierarchy.

In this work, we embrace this recursive spirit to overcome the local solver bottleneck. Instead of relying on expensive exact direct solvers or restrictive separable approximations, we propose constructing the local patch solver using a  $p$ -multigrid method (coarsening in polynomial degree) [42]. This approach applies the logic of geometric multigrid one level deeper: the local patch problem is solved iteratively by traversing a hierarchy of polynomial orders. This strategy preserves the matrix-free, sum-factorized structure of the operator at all levels, maintaining optimal memory complexity and allowing for the reuse of the global matrix-free infrastructure [2, 1].

We investigate and compare three distinct iterative strategies for the local Stokes patch problem, all underpinned by this efficient  $p$ -multigrid solver for the velocity block:

1. **Local Braess-Sarazin:** We adapt the Braess-Sarazin smoother to act as the local solver on the patch. Crucially, we employ  $p$ -multigrid to approximate the velocity inverse required within the Braess-Sarazin iteration. This effectively nests a block-smoother inside a patch-smoother inside a global multigrid cycle.
2. **Local Block GMRES:** We utilize a Krylov subspace method preconditioned with a block-triangular operator on the patch, again using  $p$ -multigrid for the velocity block.

Additionally, for Cartesian patches, we explore a block-by-block elimination approach, solving for the pressure via the Schur complement, similar to recent work on GPUs [13], but substituting exact inverses with  $p$ -multigrid approximations. Noteworthy, a high-order system can also be preconditioned by a refined mesh of degree-one elements [35], but this approach is outside the scope of our current matrix-free framework.

Our numerical results demonstrate that replacing exact local solvers with iterative  $p$ -multigrid approximations does not compromise the robustness of the global multigrid method. Specifically, the Braess-Sarazin variant proves to be exceptionally robust, handling distorted meshes and large viscosity jumps with iteration counts comparable to using exact local inverses.

The objective of this work is to establish the mathematical robustness and convergence properties of the local  $p$ -multigrid smoother. While a high-performance matrix-free implementation is the ultimate goal, this paper focuses on the algorithmic foundation and demonstrates that the 'inexact' nature of the local solver does not degrade the global convergence rate — a prerequisite for any future optimized implementation.

The paper is organized as follows. Section 2 provides the mathematical background for the Stokes problem and vertex patch smoothers. Section 2.2 describes the local solvers in detail, including the matrix-free  $p$ -multigrid framework. Section 3 presents numerical results comparing the performance of the different local solvers. For the reader interested in key performance metrics, we highlight the comparison of local solver variants in Table 1, and the global multigrid convergence results demonstrating robustness against mesh distortion and high-contrast viscosity jumps in Table 2 and Table 3, respectively. Finally, Section 4 concludes the paper.

## 2 Mathematical and Algorithmic Background

Let us first briefly describe the mathematical setup of the multigrid method, first assume a hierarchy of meshes

$$\mathbb{M}_0 \subset \mathbb{M}_1 \subset \cdots \subset \mathbb{M}_L, \quad (1)$$

subdividing a domain in  $\mathbb{R}^d$ , where the symbol “ $\subset$ ” indicates nestedness, that is, every cell of mesh  $\mathbb{M}_{\ell+1}$  is obtained from a cell of mesh  $\mathbb{M}_\ell$  by refinement. We note that topological nestedness is sufficient from the algorithmic point of view, such that domains with curved boundaries can be covered approximately.

For our numerical experiments, we consider the Stokes equations on a domain  $\Omega \subset \mathbb{R}^d$ . The weak formulation reads: find velocity  $u \in V = [H_0^1(\Omega)]^d$  and pressure  $p \in Q = L_0^2(\Omega)$  such that

$$a((u, p), (v, q)) = (\nabla u, \nabla v) - (\nabla \cdot v, p) + (\nabla \cdot u, q) = (f, v) \quad \forall (v, q) \in V \times Q. \quad (2)$$

To discretize the problem, we associate each mesh  $\mathbb{M}_\ell$  with a pair of finite element spaces  $(\mathbb{V}_\ell, \mathbb{Q}_\ell) \subset \mathbb{V} \times \mathbb{Q}$ . Specifically, we use the  $\mathbb{Q}_p - \mathbb{P}_{p-1}$  pair, which consists of continuous polynomials of degree  $p$  for the velocity and discontinuous polynomials of degree  $p-1$  for the pressure. We associate each space with its coefficient vector  $\mathbb{R}^{\dim V_\ell}$  and  $\mathbb{R}^{\dim Q_\ell}$  and do not distinguish between a finite element function and its coefficient vector by notation. Between these spaces, we introduce transfer operators

$$\begin{aligned} I_\ell^{\downarrow h} : \quad V_{\ell+1} &\rightarrow V_\ell, \\ I_\ell^{\uparrow h} : \quad V_\ell &\rightarrow V_{\ell+1}. \end{aligned} \quad (3)$$

As usual,  $I_\ell^{\uparrow h}$  is chosen as the embedding operator and  $I_\ell^{\downarrow h}$  as its  $\ell_2$ -adjoint. The subscript  $h$  indicates h-multigrid transfer between meshes of different resolution.

Note that while the finite element spaces are nested ( $V_\ell \subset V_{\ell+1}$  and  $Q_\ell \subset Q_{\ell+1}$ ), the resulting discretely divergence-free subspaces are generally non-nested. Indeed, the Stokes problem can be viewed as a symmetric positive definite problem when restricted to the space of divergence-free functions [10]. However, because our element pair does not enforce the divergence-free constraint pointwise (only a discrete divergence-free condition), the corresponding subspaces on different levels are non-nested. This is because a function being discretely divergence-free on level  $\ell$  does not automatically satisfy the more restrictive weak divergence condition on level  $\ell+1$ . True nestedness of the divergence-free subspaces is only possible when the discretization achieves an exact pointwise divergence-free condition, as is the case for certain  $H(\text{div})$ -conforming discretizations [36, 32, 3].

The discrete problem on level  $\ell$  reads

$$\mathcal{A}_\ell x_\ell = \begin{pmatrix} A_\ell & B_\ell^T \\ B_\ell & 0 \end{pmatrix} \begin{pmatrix} u_\ell \\ p_\ell \end{pmatrix} = \begin{pmatrix} f_\ell \\ 0 \end{pmatrix}, \quad (4)$$

where  $\mathcal{A}_\ell$  is the block system matrix obtained by discretization.

Multigrid methods are common solution methods for the discrete linear system (4). The efficiency of the overall method, however, depends on the choice of the so-called smoother. For saddle point problems like Stokes, constructing effective smoothers is challenging. In this work, we focus on a vertex patch smoother, which has been shown to yield robust convergence. We describe this smoother in detail in the next subsection.

---

**Algorithm 1** Application of a patch smoother where local residuals are computed on-the-fly and combined with a local solver.

---

```

function LOCAL_UPDATE(j,u)
   $u_j \leftarrow \bar{\Pi}_j u$                                  $\triangleright *Gather$ 
   $r_j \leftarrow \Pi_j b - \Pi_j \bar{A}_j u_j$            $\triangleright *Evaluate$ 
   $d_j \leftarrow \tilde{A}_j^{-1} r_j$                    $\triangleright *Solve$ 
  return  $\Pi_j^T d_j$                                  $\triangleright *Scatter$ 
end function

for  $j = 1, \dots, N_{\text{patches}}$  do                 $\triangleright$  Main smoother sweep
   $u \leftarrow^+ \text{LOCAL\_UPDATE}(j,u)$ 
end for

```

---

## 2.1 Vertex patch smoothers

The vertex patch smoother is an overlapping subspace correction method [3, 19, 21, 47, 8, 46]. The domain is decomposed into a collection of overlapping subdomains, or *patches*  $\Omega_j$ , each formed by the cells surrounding an interior vertex. The smoother iteratively improves the solution by solving local problems on these patches. We employ a multiplicative (Gauss-Seidel-like) variant, where patches are processed sequentially.

The update for a single patch  $j$  consists of four main steps. To define these, we introduce restriction operators:  $\bar{\Pi}_j$  extracts all degrees of freedom (DoFs) on a patch  $\Omega_j$  (including its boundary) from a global vector, while  $\Pi_j$  extracts only the DoFs interior to the patch.

1. **Gather.** Collect the current solution values on the patch into a local vector:  $\bar{u}_j = \bar{\Pi}_j u$ .
2. **Evaluate.** Compute the local residual  $r_j$  for the interior DoFs. This uses the local operator  $\bar{A}_j$  (acting on all patch DoFs) and the global right-hand side  $b$ :  $r_j = \Pi_j b - \Pi_j \bar{A}_j \bar{u}_j$ .
3. **Local solve.** Find a correction  $d_j$  by approximately solving the local system on the patch interior:  $d_j \approx \tilde{A}_j^{-1} r_j$ , where  $\tilde{A}_j^{-1}$  is an inexpensive approximate solver.
4. **Scatter.** Add the local correction  $d_j$  back to the global solution vector using the transpose of the interior restriction operator:  $u \leftarrow^+ \Pi_j^T d_j$ .

These steps are summarized in Algorithm 1. This implementation follows the cell-oriented loop structure proposed in [46], which is well-suited for matrix-free operator evaluation.

In this work, we focus on the local solve (step 3), which is critical for the overall performance. This step, denoted as the application of an approximate inverse  $\tilde{A}_j^{-1}$  in Algorithm 1, is performed by applying a few iterations of a preconditioned Richardson method, as outlined in Algorithm 2. Notice that the first iteration is performed outside the loop to avoid an unnecessary matrix-vector product, since the initial guess for the correction is zero.

## 2.2 Local Solvers for Stokes Patch Problems

The efficiency of the patch smoother hinges on the local solve step. For the Stokes equations, this involves solving a saddle point system on each patch. We consider three iterative approaches for this task: the Braess-Sarazin smoother, a block GMRES solver, and a block-by-block approach using the Schur complement.

---

**Algorithm 2** Local preconditioned Richardson iteration for the patch problem. This function implements the action of  $\tilde{A}_j^{-1}$  from Algorithm 1.

---

```

1: function LOCALSOLVE( $r_j$ )                                 $\triangleright$  The input  $r_j$  is the residual for the patch problem.
2:    $d_j \leftarrow \text{P-V-CYCLE}(r_j)$                           $\triangleright$  First iteration with zero initial guess.
3:   for  $k = 2, \dots, N_{\text{iter}}$  do                          $\triangleright$  Apply remaining steps.
4:      $\text{res} \leftarrow r_j - A_j d_j$                           $\triangleright$  Compute residual for the correction.
5:      $c_j \leftarrow \text{P-V-CYCLE}(\text{res})$                     $\triangleright$  Precondition with one p-MG cycle.
6:      $d_j \leftarrow c_j$                                           $\triangleright$  Update correction.
7:   end for
8:   return  $d_j$ 
9: end function

```

---

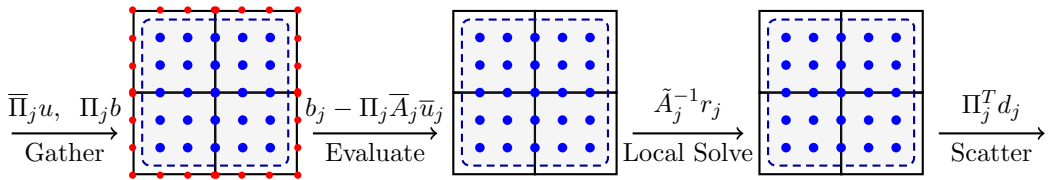


Figure 1: Workflow in a generic smoother application of a patch smoother for a single patch  $j$ . The three panels represent the main steps: gathering data from the global solution and right-hand side, computing the local residual, and applying the local correction and scattering it back to the global solution. Blue dots indicate interior DoFs of the patch, while red dots indicate all DoFs (including boundary) associated with each cell. The dashed rectangle highlights the patch interior. Figure taken from [43].

All these methods rely on a local multigrid solver. Since a patch contains too few cells for effective geometric coarsening, we construct a hierarchy of levels by reducing the polynomial degree  $p$ . This p-multigrid approach, detailed in [42], provides an effective and computationally efficient way to approximate the action of the inverse. It is computationally inexpensive to apply while keeping memory requirements low by relying on matrix-free data structures and storing only compact per-patch data.

We distinguish between two main ways to employ this local p-multigrid solver:

1. **Multigrid on the Stokes System (Braess-Sarazin):** The p-multigrid V-cycle is applied to the full Stokes system  $M_j$ . The smoother on each level is the Braess-Sarazin iteration.
2. **Multigrid on the Velocity Block (Block Solvers):** The p-multigrid V-cycle is applied only to the velocity block  $A_j$  to approximate its inverse. This approximate inverse is then used within a block preconditioner for the full system.

### 2.2.1 Local p-Multigrid Framework

To solve a local patch problem  $M_j d_j = r_j$ , where  $M_j$  is either the full Stokes system or the velocity block  $A_j$ , we employ a p-multigrid method. As with any multigrid method, the p-multigrid solver is built upon a few key components: a hierarchy of levels, transfer operators between these levels, a smoother  $S_{j,p}$  (with relaxation parameter  $\omega$  and  $m$  steps) and operator  $M_{j,p}$  on each level, and a coarse-grid solver.

In the p-multigrid context, the levels correspond to a hierarchy of polynomial degrees. We choose a geometric progression, such as  $p_l = 1, 3, 7, \dots$ , up to the target degree. If the target

degree does not fit this sequence, the hierarchy is adjusted accordingly; for instance, for a target degree of  $p = 4$ , the sequence would be 1, 3, 4. The transfer operators are the natural embedding for prolongation (from degree  $p_{l-1}$  to  $p_l$ ) and its adjoint for restriction. The explicit Kronecker product structure of these operators and the closed-form definitions of the level operators are detailed in Appendix A.

The complete p-multigrid V-cycle is outlined in Algorithm 3 in which we also include the option for skipping the post-smoothing step. The algorithm recursively descends to the coarsest level, where an exact solve is performed.

---

**Algorithm 3** The p-multigrid V-cycle for a local patch problem. The post-smoothing step (lines 12-13) is omitted in the *half V-cycle* optimization.

---

```

1: function V-CYCLE( $l, r_p$ )
2:   if  $l = 1$  then
3:      $d_1 \leftarrow M_{j,1}^{-1} r_1$                                  $\triangleright$  Coarse-level solve
4:     return  $d_1$ 
5:   end if
6:    $d_p \leftarrow \omega S_{j,p}^{-1} r_p$                           $\triangleright$  Pre-smoothing
7:    $\text{res}_p \leftarrow r_p - M_{j,p} d_p$                        $\triangleright$  Compute residual
8:    $\text{res}_{p-1} \leftarrow I_{p,p-1}^{\downarrow p} \text{res}_p$          $\triangleright$  Restrict residual
9:    $e_{p-1} \leftarrow \text{V-CYCLE}(p-1, \text{res}_{p-1})$            $\triangleright$  Recursive call
10:   $e_p \leftarrow I_{p-1,p}^{\uparrow p} e_{p-1}$                        $\triangleright$  Prolongate correction
11:   $d_p \leftarrow d_p + e_p$                                       $\triangleright$  Apply correction
12:  if full V-cycle then
13:     $\text{res}_p \leftarrow r_p - M_{j,p} d_p$                        $\triangleright$  Compute residual for post-smoothing
14:     $d_p \leftarrow d_p + \omega S_{j,p}^{-1} \text{res}_p$            $\triangleright$  Post-smoothing
15:  end if
16:  return  $d_p$ 
17: end function

```

---

### 2.2.2 Multigrid on the Stokes System

In this approach, we apply multigrid to the entire Stokes problem on the patch. As with any geometric or p-multigrid method, the efficiency of the solver relies on three ingredients: the transfers and level operators, the coarse grid solver, and the smoother.

The definition of the level systems and transfer operators is standard. The level operators correspond to the discretization of the Stokes problem using the finite element space of polynomial degree  $p$  associated with the current level. The transfer operators are the natural embeddings between the nested velocity and pressure spaces and their adjoints.

The coarse grid solver, however, requires special consideration. The hierarchy of levels bottoms out at  $p = 1$ . While the velocity space is defined on the mesh of the patch, we define the pressure space on a coarsened geometry; treating the entire patch as a single macro-cell (e.g., a single square instead of the four cells that typically form a 2D patch). This choice results in a pressure space consisting of only a single constant degree of freedom over the whole patch. Since we solve local problems with homogeneous Dirichlet boundary conditions for the velocity, the pressure is only defined up to a constant. To ensure a unique solution, we fix the average pressure on the patch to zero. However, enforcing a zero mean on a space of constants constrains the single available degree of freedom to be zero. Consequently, the effective pressure space on the coarsest level is empty,

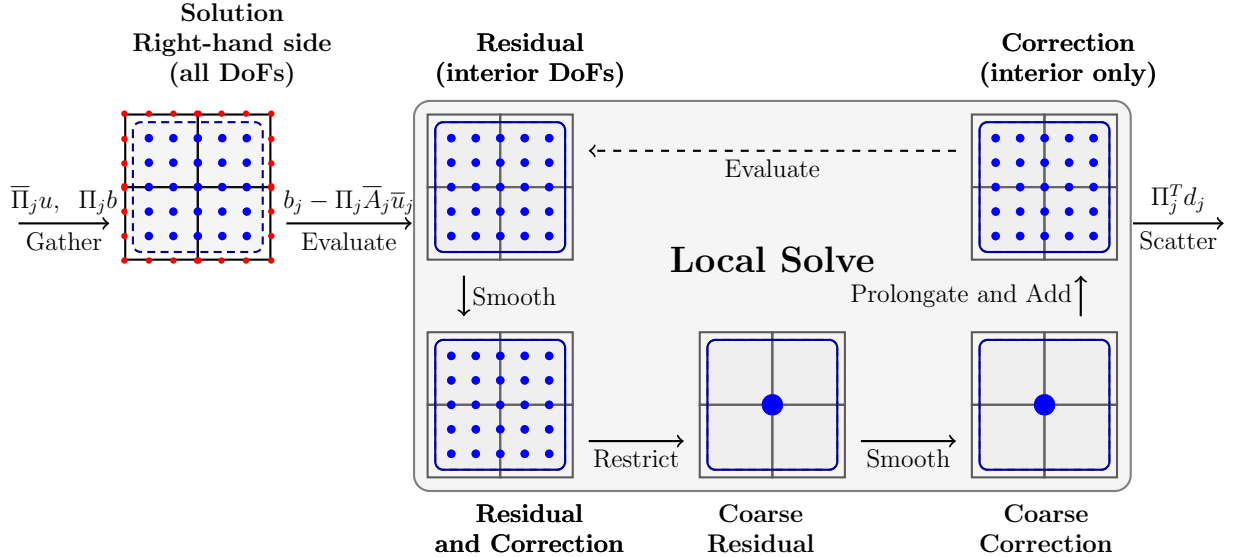


Figure 2: Patch-smoother data flow for a local p-multigrid solve (illustration for  $p = 3$  on the fine local level). The coarse level shown is  $p = 1$  and contains a single interior node. The diagram shows gather, evaluate (local residual), pre-smoothing, restriction to the coarse level, an exact coarse correction, prolongation-and-add, and scatter-add. A dashed arrow indicates proceeding to the next local multigrid iteration. For brevity we illustrate only pre-smoothing; post-smoothing is omitted. Figure taken from [43].

and the coarse grid solve reduces to a symmetric positive definite problem for the velocity variables only.

For the smoother  $S_{j,p}$  on the levels  $p > 1$ , we employ the Braess-Sarazin smoother [6]. Use of this smoother is motivated by its robustness with respect to the stationary or non-stationary nature of the flow. Each smoothing step involves solving the saddle point system

$$\begin{pmatrix} \tilde{A}_j & B_j^T \\ B_j & 0 \end{pmatrix} \begin{pmatrix} \delta u_j \\ \delta p_j \end{pmatrix} = \begin{pmatrix} r_{u,j} \\ r_{p,j} \end{pmatrix}, \quad (5)$$

where  $\tilde{A}_j$  is a symmetric positive definite approximation of the velocity block  $A_j$ . This system is solved using block-wise elimination, which proceeds in three stages:

1. Compute an intermediate velocity correction:  $\delta u_j^{(1)} = \tilde{A}_j^{-1} r_{u,j}$ .
2. Solve the Schur complement system for the pressure correction  $\delta p_j$ :

$$S_j \delta p_j = B_j \delta u_j^{(1)} - r_{p,j}, \quad \text{with } S_j = B_j \tilde{A}_j^{-1} B_j^T. \quad (6)$$

3. Perform the final velocity update:  $\delta u_j = \delta u_j^{(1)} - \tilde{A}_j^{-1} B_j^T \delta p_j$ .

The resulting smoothing operator is denoted by  $\mathcal{S}_k^{-1}$  and its closed-form block representation is presented in Appendix A.

The effectiveness of the Braess-Sarazin smoother relies on one of two conditions[50]: either  $\tilde{A}_j$  is a high-quality preconditioner for  $A_j$ , or the Schur complement system (6) is solved accurately. In this work, we follow the latter approach. The classical method proposed by Zulehner [50] ensures

robustness by solving the Schur complement system with a multigrid method. However, it has been shown in [44] that even a single iteration of a standard iterative solver like the Conjugate Gradient (CG) method can be sufficient to maintain robust convergence, which significantly reduces the computational overhead of the local solve.

We evaluate two options for the inner solver used to solve the Schur complement system (6): CG and Richardson iteration. We denote the number of inner iterations by  $n_S$ . While CG is typically more efficient in terms of iteration counts, it is a non-linear operator. Its use within the smoother requires the outer Krylov solver to be flexible (e.g., FGMRES). In contrast, Richardson iteration is a linear operator and preserves the consistency of the preconditioner. Furthermore, Richardson iteration offers a specific computational benefit: for a zero initial guess, the first iteration does not require an evaluation of the Schur operator  $S_j$ . Since  $S_j$  involves two applications of  $B$  and one of  $\tilde{A}_j^{-1}$ , skipping this evaluation for the first step provides a meaningful speedup. When Richardson iteration is used, its relaxation parameter is autotuned based on an eigenvalue estimate of the preconditioned operator to ensure stability and rapid convergence.

Both inner solvers are preconditioned with an approximation  $\tilde{S}_j^{-1}$  of the inverse Schur complement, which we typically choose as the (approximate) diagonal of  $S_j$ . If  $\tilde{A}_j$  is chosen as the diagonal of  $A_j$  (damped Jacobi), the exact diagonal of  $S_j$  can be computed. Even if  $\tilde{A}_j$  is not diagonal, an effective preconditioner can be constructed by approximating  $\tilde{A}_j^{-1}$  with  $(\text{diag}(A_j))^{-1}$  when computing the Schur diagonal, as shown in [44]. Although more advanced approximations for  $\tilde{A}_j^{-1}$  are possible (e.g., using Chebyshev polynomials or scaling with eigenvalue estimates), we focus here on simple diagonal approximations.

We note a special case for Cartesian grids where the Fast Diagonalization Method (FDM) allows for the exact inversion of  $A_j$  at low cost. In this scenario, one could technically use  $\tilde{A}_j = A_j$  combined with a less accurate Schur solver. This would resemble a block preconditioner approach but applied within the multilevel hierarchy. However, since our focus is on general unstructured patches where FDM is not available, we do not pursue this direction further.

Additionally, the choice for the number of smoothing steps  $m$  per level is motivated by theory. The analyses in [6, 50] are formulated for nested multigrid cycles with at least two smoothing steps (pre- and post-smoothing) per level, i.e.,  $m = 2$ ; these hypotheses underpin the theoretical robustness results. In practice, however, one can try using a single smoothing step ( $m = 1$ ) to reduce cost. Therefore we explicitly test both variants in our experiments: the two-step (classical) smoother that matches the theory, and the single-step (economized) variant that omits post-smoothing. The single-step variant may weaken the strict theoretical guarantees but can offer substantial runtime savings, and in our numerical tests it typically leads to only a modest increase in outer iteration counts for the Braess–Sarazin approach.

An additional advantage of the Braess–Sarazin smoother is its robustness with respect to the specific form of the equation, maintaining effectiveness for stationary Stokes, non-stationary variants, and even linearized operators like the Oseen equations [45]. While convergence rates may vary depending on the flow regime, the smoother’s block-wise structure naturally balances mass and stiffness contributions, whereas some block preconditioners can be more sensitive to the relative weighting of these terms [33].

### 2.2.3 Block Solvers: Multigrid on the Velocity Block

Alternatively, we can employ an iterative solver, such as GMRES with a block preconditioner, for the local Stokes system. In this case, the p-multigrid method is used solely to approximate the inverse of the velocity block  $A_j$ . To ensure symmetry and robustness, we use a symmetric block

preconditioner  $\mathcal{P}_j$  that mirrors the structure of the Braess-Sarazin iteration:

$$\mathcal{P}_j^{-1} = \begin{pmatrix} \tilde{A}_j & B_j^T \\ B_j & 0 \end{pmatrix}^{-1} \quad (7)$$

where  $\tilde{A}_j^{-1}$  is a high-quality approximation of the velocity inverse, typically obtained by one or more p-multigrid V-cycles (setting  $M_j = A_j$  in Algorithm 3). Similarly,  $\tilde{S}_j^{-1}$  is a *good* approximation of the inverse Schur complement, for instance, the action of a pressure mass matrix inverse or a simple iterative solve.

The advantage of GMRES is its ability to handle the indefinite nature of the saddle point system without requiring an exact Schur complement solve. However, the downside is that the structure of the preconditioner is problem-dependent, and with variable coefficients or non-stationary flows, its performance can degrade. In that case, a better approximation of the Schur complement can be obtained by including a weighted inverse mass matrix and inverse laplacian operator [33]. Since laplacian inverses are not easily available in our patch setting, another p-multigrid V-cycle could be used to approximate the laplacian inverse on the pressure space. However, this would significantly increase the computational cost of the local solve, and we do not pursue this direction further.

#### 2.2.4 Blockwise Elimination via Schur Complement

Finally, we consider a block-by-block iteration based on the Schur complement. This method follows the same three-stage elimination procedure described for the Braess-Sarazin smoother in Section 2.2.2, with the specific choice  $\tilde{A}_j = A_j$ , i.e., using the exact inverse of the velocity block. This approach, which has also been successfully utilized in [13], is primarily feasible on Cartesian grids where the Fast Diagonalization Method (FDM) [27] allows for the exact inversion of  $A_j$  at a computational cost comparable to a few matrix-vector products.

A significant challenge, even in this ideal Cartesian setting, remains the lack of a *silver bullet* for the Schur complement  $S_j = B_j A_j^{-1} B_j^T$  comparable to FDM for the Poisson equation. While the Laplacian on a Cartesian patch can be decomposed into a Kronecker product of 1D operators to enable an  $O(N^{d+1/d})$  solve, the Stokes Schur complement does not inherit this separable structure. The coupling between velocity components and the divergence constraint breaks the separability required for FDM. Consequently, one must either rely on the explicit formation of the (dense) Schur complement matrix which is only practical for low polynomial degrees, or use iterative solvers to obtain the pressure. In [13] an average of 15 CG iteration on Schur complement was reported. For general unstructured or distorted patches where FDM is unavailable, the requirement of an exact velocity inverse would make this block-by-block approach significantly more expensive than the standard Braess-Sarazin iteration, further motivating our use of p-multigrid to approximate the velocity inverse.

#### 2.2.5 Summary of local solver variants

The two iterative approaches Presented above (Braess-Sarazin and block solvers) share a common architectural framework and are configured by the following tuning parameters:

- the **number of smoothing steps**  $m$  and the **relaxation parameter**  $\omega$  used within the local p-multigrid levels (applied to either the full Stokes system or the velocity block);
- the **velocity block approximation**  $\tilde{A}_j^{-1}$ , ranging from a simple diagonal or damped Jacobi step to p-multigrid V-cycles or an exact inverse; in case if p-multigrid is used, then relaxation parameter  $\omega$  and number of smoothing steps  $m$  per level must be specified.

- the **Schur complement approximation**  $\tilde{S}_j^{-1}$ , typically chosen as a (preconditioned) diagonal or a pressure mass matrix inverse  $\mathcal{M}_p^{-1}$ .

For Braess–Sarazin the following additional parameters are considered:

- the **Schur solver**, either preconditioned CG or Richardson iteration;
- the **number of inner iterations**  $n_S$  for the Schur complement solve.

Unless stated otherwise, we use  $m = 1$  smoothing step per level and  $n_S = 1$  inner Richardson iteration for the Schur complement in the Braess–Sarazin solver. We emphasize that when Richardson iteration is used for the Schur system, the relaxation parameter is autotuned via an eigenvalue estimate of the preconditioned operator  $\tilde{S}_j^{-1}S_j$ . In all experiments, we choose the damping parameter  $\omega = 0.7$ . Interestingly, the approximate local inverse obtained via a single p-multigrid V-cycle with one smoothing step per level can be written in closed form as a combination of Kronecker products; we provide the explicit formulas in Appendix A.

### 3 Numerical results

In this section, we present a series of numerical experiments to evaluate the performance of the proposed local p-multigrid solvers and their effectiveness as smoothers in a global geometric multigrid hierarchy for the Stokes equations. We begin by validating the local solvers on a single patch, allowing us to isolate their convergence properties from the global multigrid components and assess their sensitivity to mesh distortion and coefficient variation. Subsequently, we incorporate these local solvers into a full geometric multigrid framework and investigate the overall solver efficiency for various problem configurations.

All tests are conducted using a homogeneous right-hand side ( $f = 0$ ) and a random initial guess, which provides a representative test for the smoothing properties across all frequency modes. We note that the current experimental implementation is based on sparse matrix data structures to facilitate development (and consequently, debugging). While this choice allows for rapid prototyping of different local solver variants, it does not reflect the peak performance achievable with a fully optimized matrix-free implementation. Consequently, our performance metrics focus primarily on iteration counts and relative convergence rates rather than absolute runtimes, which would be significantly lower in a production-ready matrix-free environment.

#### 3.1 Numerical validation on a single patch

Before integrating the local p-multigrid solver into the global smoothing procedure, we first evaluate its performance on a single vertex patch. This validation section follows the methodology presented in [42] for the scalar Laplace problem, which we adapt here for the Stokes equations. For these tests, we run the FGMRES solver using a p-multigrid V-cycle as a preconditioner until the relative residual is reduced below a tolerance of  $10^{-8}$ . We emphasize that such a stringent tolerance is not necessary when the p-multigrid is used as a patch smoother in the global algorithm: a much looser tolerance typically suffices and is computationally cheaper. We nevertheless enforce  $10^{-8}$  here to increase the number of FGMRES iterations, which makes convergence behavior easier to inspect and provides more detailed diagnostics for validation. These tests are not intended to validate the local solver as a standalone production solver; rather, they isolate its behaviour from other multigrid components and assess only the contributions proposed in this paper.

We evaluate the performance of various local solver variants on a single vertex patch consisting of  $2^d$  cells in spatial dimensions  $d = 2$  and  $d = 3$ . Following [42], we also test simplicial (unstructured)

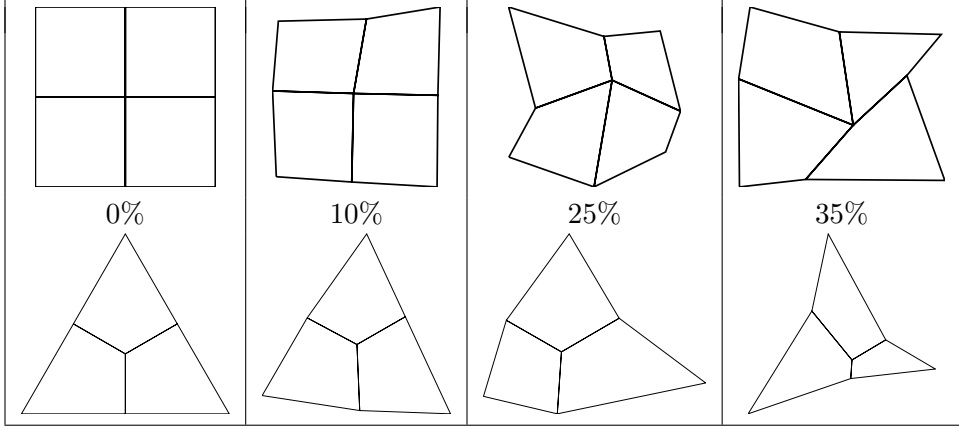


Figure 3: Illustration of the vertex-based patches used in our 2D experiments. The top row shows structured (Cartesian) patches, while the bottom row depicts unstructured (simplicial) patches. The distortion level  $\delta$  represents the maximum displacement of each interior vertex relative to the local mesh size  $h$ .

patches comprising 3 quadrilaterals in 2D or 4 hexahedra in 3D; representative geometries are shown in Figure 3. Our investigation starts with the Stokes problem on an undeformed Cartesian patch as a baseline and progressively increases difficulty to probe the robustness and limitations of the proposed methods.

The first level of complexity involves geometric distortion introduced by randomly displacing each vertex. As in [42], each interior vertex is shifted by a vector of length  $\delta h$ , with its direction sampled uniformly on the unit sphere  $S^{d-1}$ . For larger distortions, generated patches may contain degenerate elements with concave or inverted corners. For 2D Cartesian patches, degeneracy occurs when the distortion exceeds  $\delta = \frac{1}{2} \frac{\sqrt{2}}{2} \approx 0.3535$ , while in 3D the threshold is  $\delta = \frac{1}{2} \frac{\sqrt{3}}{3} \approx 0.2887$ . Accordingly, we test distortions up to 35% in 2D and 30% in 3D. We note that simplicial patches exhibit higher sensitivity to distortion because the initial angles already exceed  $90^\circ$ , causing some cells to approach triangular shapes with angles near  $180^\circ$ .

Secondly, we investigate the influence of heterogeneous material properties, focusing on discontinuous viscosity jumps where one cell carries a large contrast relative to others. Finally, we combine geometric deformation and strong coefficient variation to evaluate the solvers under extreme conditions, considering both stationary and non-stationary flow regimes. For each scenario, we report FGMRES iteration counts (to a tolerance of  $10^{-8}$ ) across a range of polynomial degrees  $p$ . Following the findings in [42], where 2D and 3D results were shown to be qualitatively similar, we focus most experiments on the 2D case to save computational resources and present 3D results only for selected configurations.

We perform 20 independent random realizations when testing geometric distortion and report the average number of iterations over all runs. Each local solve is allowed a maximum of 150 iterations; if a run does not reach the convergence tolerance within this limit, it is declared non-convergent. Such runs would be assigned a large sentinel iteration count to make non-convergence immediately apparent.

**Convergence on Cartesian Patches** We begin by evaluating the baseline performance of the various local solvers on undeformed Cartesian patches with a constant coefficient. In this setting, the velocity block  $A_j$  can be inverted exactly using the Fast Diagonalization, providing a reference

case for evaluating the impact of different approximations for the velocity and Schur complement blocks.

We compare five different variants: (i) the Braess–Sarazin smoother using a diagonal approximation  $\tilde{A}_j^{-1}$  and an inner Richardson iteration for the Schur complement; (ii) Braess–Sarazin using the same  $\tilde{A}_j^{-1}$  but with a single CG iteration for the Schur system; (iii) a block GMRES solver using the exact velocity inverse and a pressure mass matrix  $\mathcal{M}_p^{-1}$  for the Schur contribution; (iv) block GMRES where the velocity block is instead approximated by a single  $p$ -multigrid V-cycle; and (v) the blockwise elimination approach using the exact velocity inverse and an iterative CG solve for the Schur complement. Table 1 summarizes the number of FGMRES iterations required for convergence as a function of the polynomial degree  $p$ .

We observe that the Braess–Sarazin variants demonstrate remarkable robustness: even with the simple diagonal approximation for the velocity block, they consistently outperform the block-based solvers. For instance, with  $m = 2$  smoothing steps, the Braess–Sarazin iteration counts are nearly a factor of two lower than those of the block GMRES and blockwise elimination methods, even when the latter are equipped with the exact inverse  $A^{-1}$ . Under these ideal Cartesian conditions, the CG-based and Richardson-based inner Schur solvers for Braess–Sarazin yield virtually identical iteration counts.

In contrast, the performance of the block GMRES solver is highly sensitive to the quality of the velocity inverse. While the iteration counts are stable when  $A^{-1}$  is inverted exactly, substituting it with a single  $p$ -multigrid V-cycle (variant iv) leads to a significant degradation in performance, with the iteration count rising sharply as the polynomial degree  $p$  increases.

We note that the iteration counts exhibit characteristic non-monotonic behavior, with visible drops at  $p = 4$  and  $p = 8$ . This is an artifact of the  $p$ -multigrid level structure used in the hierarchy, an effect previously analyzed for the scalar case in [42]. We build  $p$ -levels using the nested sequence 1, 3, 7, 15, etc. (i.e.,  $p_{k+1} = 2p_k + 1$ ). Degrees that are just above these nodes benefit from a more complete multigrid hierarchy; for example, for  $p = 7$  the hierarchy is simply  $\{1, 3, 7\}$ , whereas for  $p = 8$  it becomes  $\{1, 3, 7, 8\}$ , effectively yielding a method closer to performing two smoothing steps on the finest level.

Table 1: Number of iterations for solving the local Stokes problem on a 2D Cartesian patch. Comparison of Braess–Sarazin with two variants of Schur solver: Richardson and CG, Block GMRES with exact velocity inverse and  $p$ -multigrid velocity inverse, and blockwise elimination with exact velocity inverse.

Method	$\tilde{A}^{-1}$	$\tilde{S}^{-1}$	$m$	Polynomial Degree $p$						
				2	3	4	5	7	8	11
Braess–Sarazin	$\omega \text{diag}(A)^{-1}$	$\text{diag}(\hat{S}^{-1})$	1	6	9	8	9	13	10	13
			2	4	6	6	6	9	7	9
	1 PCG it.	1	6	10	8	9	13	10	13	
		2	4	6	6	6	9	7	9	
Block GMRES	p-MG V-cycle	$M_p^{-1}$	1	15	28	33	38	52	45	57
			2	13	24	27	31	39	37	44
	$A^{-1}$	$M_p^{-1}$	–	9	14	16	17	18	19	20
Blockwise Elm.	$A^{-1}$	CG	–	8	14	16	18	21	22	22

**Resilience to Geometric Distortion** Next, we examine the solver’s performance under geometric perturbations. We apply a random, nonlinear distortion to the patch geometry controlled by a *distortion* parameter  $\delta$ , with zero corresponding to an undeformed patch. Figure 4 presents the results for the block GMRES solvers used as a baseline for comparison. Here, the local Stokes problem is solved using a block preconditioner where the velocity block  $A$  is approximated by either a single  $p$ -multigrid V-cycle (solid lines) or its exact inverse (dashed lines). The left and right panels show results for 2D and 3D, respectively. For small distortions, the iteration counts are stable across all polynomial degrees. However, as the distortion increases, the performance depends on the spatial dimension and the polynomial degree. In 2D, the iteration count grows moderately, and the gap between the  $p$ -multigrid approximation and the exact inverse remains small. In 3D, the block solver is significantly more sensitive: for higher polynomial degrees such as  $p = 7$ , the iteration counts rise faster with distortion.

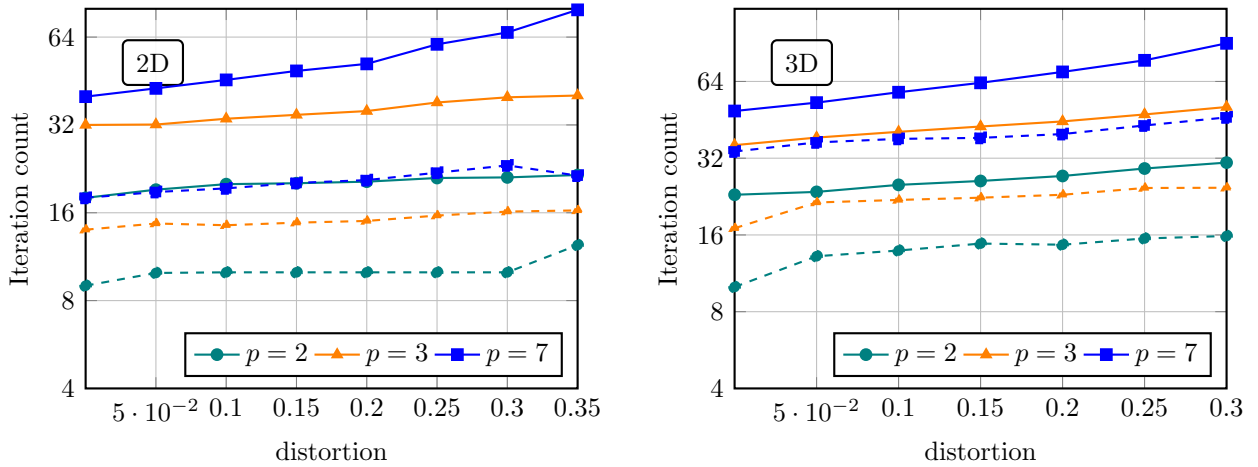


Figure 4: Number of FGMRES iterations (logarithmic y-axis) vs. mesh distortion for local block solver on structured patches in 2D (left) and 3D (right). Solid lines: velocity block  $A$  is approximated via a single  $p$ -multigrid V-cycle; dashed lines: exact velocity inverse; dotted lines: reference.

We now contrast these baseline results with the Braess–Sarazin smoother, which is our primary focus. In Figure 5, we show the iteration counts (again on a logarithmic scale) for the  $p$ -multigrid solver using Braess–Sarazin smoothing. Figure 5 shows the iteration counts for the Braess–Sarazin smoother using one smoothing step per level ( $m = 1$ ). We compare structured patches (solid lines) with unstructured simplex patches (dashed lines). In 2D (left panel), the Braess–Sarazin smoother demonstrates remarkable robustness, with iteration counts remaining below 20 even for 35% distortion, showing almost no dependence on the polynomial degree. The only exception is the highest polynomial degree  $p = 7$  on simplicial patches, where the solver failed to converge for some realizations with large distortion  $\delta = 0.3$ . In 3D (right panel), while iteration counts are slightly higher, they remain stable and significantly more efficient than the block solvers from Figure 4. Notably, the Braess–Sarazin smoother handles both structured and simplicial patches with similar efficiency, and the performance degradation observed for high  $p$  in 3D is much less pronounced here. This suggests that the saddle-point coupling in the Braess–Sarazin approach is better suited for distorted patches than the decoupled block-preconditioning approach. We also compare the results with those for the scalar Poisson problem on structured patches (dotted lines) from [42], which shows similar trends while requiring slightly fewer iterations.

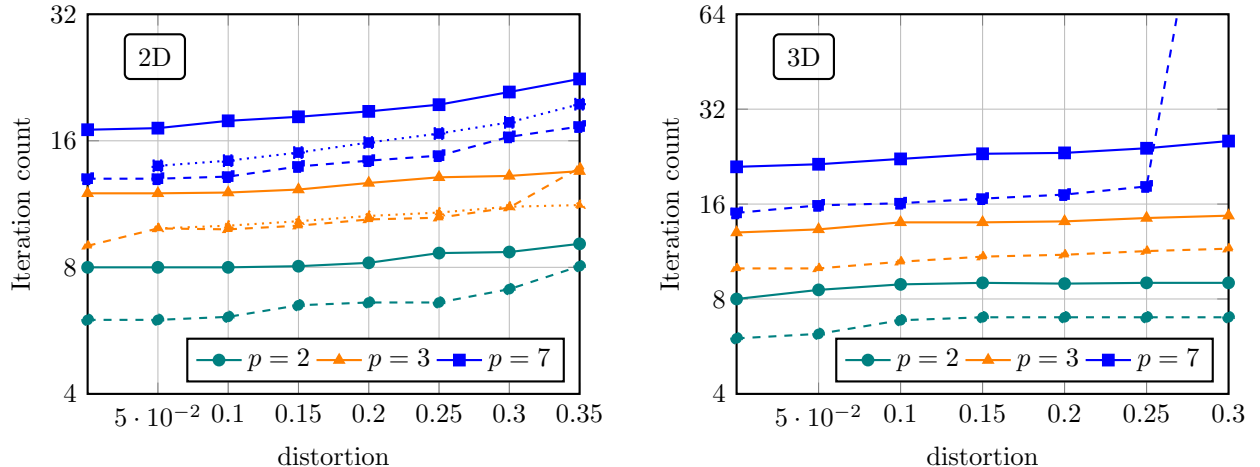


Figure 5: Number of FGMRES iterations (logarithmic y-axis) vs. mesh distortion for Braess–Sarazin smoother on structured patches. Both variants use one smoothing step per level. Solid lines: structured patch, dashed lines: simplicial patch, dotted lines: reference Poisson problem iteration counts (available for  $p = 3$  and  $p = 7$ ). Left subplot: 2D; right subplot: 3D. For  $p = 7$  the solver did not converge in some runs with  $\delta = 0.3$  on simplicial patches. Dotted lines: reference Poisson problem iteration counts (available for  $p = 3$  and  $p = 7$  in 2D)

**Viscosity Jumps and Non-Zero Density** We now investigate robustness to variations in the material coefficient, focusing on a challenging discontinuous jump. In this test, one cell in the patch is assigned a coefficient  $\mu$  while all other cells have coefficient 1. Figure 6 presents two related experiments in 2D using the Braess–Sarazin smoother. The left panel plots the number of iterations (shown on a logarithmic y-axis) against the magnitude of the coefficient jump  $\mu$  on an undeformed patch. The Braess–Sarazin smoother (solid and dashed lines for Cartesian and simplex patches, respectively) demonstrates excellent robustness, with iteration counts showing only a minimal increase as the jump magnitude grows from  $10^0$  to  $10^8$ . In this configuration, the block GMRES solver (dotted lines), which utilizes the pressure mass matrix inverse  $M_p^{-1}$  as a preconditioner for the Schur complement, also maintains stable performance. While it requires roughly twice as many iterations as the Braess–Sarazin approach, it does not exhibit any severe degradation as the jump magnitude increases. These results suggest that Braess–Sarazin remains the more efficient and consistent choice across varying degrees of numerical difficulty, providing significant acceleration compared to the simpler decoupled block-preconditioning approach.

The right panel of Figure 6 examines the combined challenge of geometric distortion and a large coefficient jump. It shows the iteration counts for a 2D patch with a fixed jump  $\mu = 10^4$  as the distortion increases. By comparing these results with the constant-coefficient case (Figure 5), we observe that the presence of the jump has a negligible effect on the Braess–Sarazin solver’s sensitivity to distortion. However, the block solver (dotted lines) did not converge for  $p = 7$  when distortion reached 35%. This level of robustness is critical for practical applications where complex geometries and heterogeneous materials are often encountered together.

Finally, we evaluate the solver’s robustness for the non-stationary Stokes equations by setting the density  $\rho = 1$  (Figure 7). The results for the Braess–Sarazin smoother (solid lines) are qualitatively similar to the stationary case, with excellent robustness to both viscosity jumps and mesh distortion. In this non-stationary regime, the block GMRES solver (dotted lines) also demonstrates stable performance across the entire range of viscosity contrasts, although it fails to converge for high

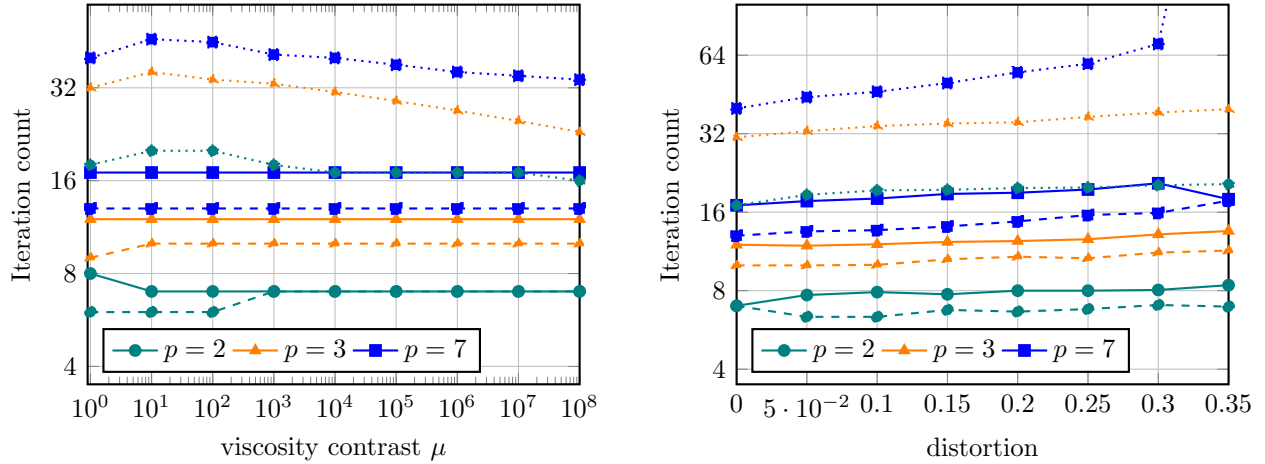


Figure 6: Solver iterations (logarithmic y-axis) vs. coefficient jump and mesh distortion (Stationary case,  $\rho = 0$ ). Left panel: FGMRES iterations on an undeformed 2D patch as the coefficient jump  $\mu$  varies. Right panel: FGMRES iterations on a 2D patch with a fixed coefficient jump  $\mu = 10^4$  as the mesh distortion increases. Solid lines: structured patches; dashed lines: Simplex patches; dotted lines: block solver. In both panels, we use p-multigrid with Braess–Sarazin smoother and one smoothing step per level. For  $p = 7$  the block solver did not converge in some runs with  $\delta = 0.35$ .

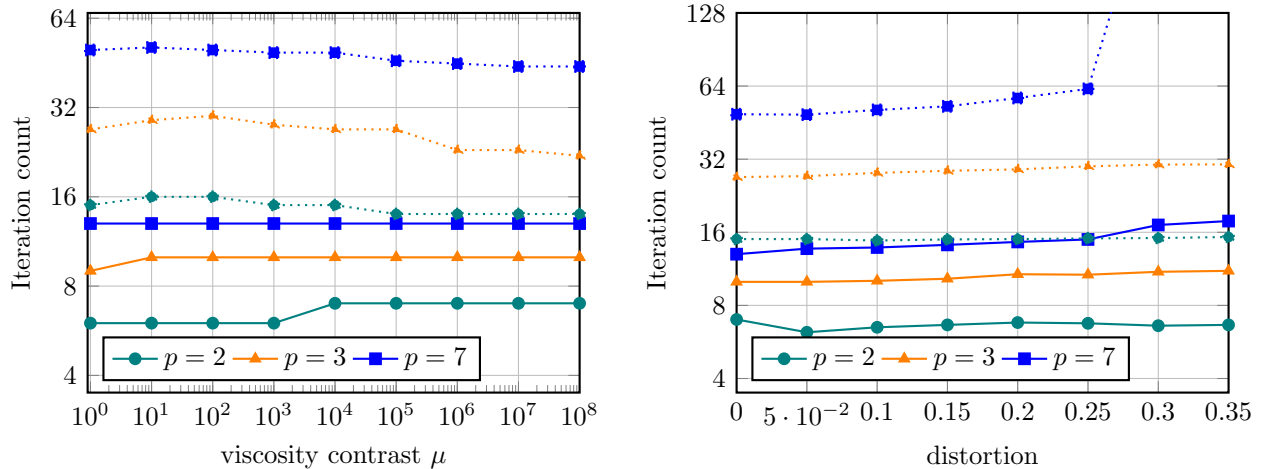


Figure 7: Solver iterations (logarithmic y-axis) vs. coefficient jump and mesh distortion for non-stationary Stokes ( $\rho = 1$ ). Left panel: iterations on an undeformed 2D structured patch as viscosity jump  $\mu$  varies. Right panel: iterations on a 2D structured patch with fixed jump  $\mu = 10^4$  and increasing distortion. Solid lines: Braess–Sarazin smoother; dotted lines: block solver. Both variants use p-multigrid for the velocity block. For  $p = 7$  the block solver did not converge in some runs with  $\delta \geq 0.3$ .

polynomial degrees ( $p = 7$ ) when the patch distortion exceeds 30%. While it requires approximately twice as many iterations as the Braess–Sarazin approach, it avoids the typical convergence issues associated with strong coefficient jumps on less distorted meshes. Notably, the iteration counts for the block solver are nearly identical to those observed in the stationary case, indicating that the addition of the mass term in the velocity block does not significantly alter the solver’s asymptotic behavior with respect to the jump magnitude in this configuration. As in the stationary case, the block solver baseline uses  $M_p^{-1}$  to approximate the Schur complement inverse; although there is room for further improvement through more advanced Schur preconditioners, Braess–Sarazin remains the more efficient choice for rapid and consistent convergence.

**Summary** Our numerical study on single patches demonstrates that the local p-multigrid solver using the Braess–Sarazin smoother is a highly robust and versatile choice. It maintains stable performance across a wide range of mesh distortions, spatial dimensions, and extreme coefficient jumps, making it well-suited for the complex conditions encountered in practical Stokes flow simulations. While its iteration counts show some sensitivity to the polynomial degree  $p$  and the mesh distortion, the degradation is much more graceful than the decoupled block-preconditioning approaches. The performance gap is clearly visible in the logarithmic plots shown in Figures 6 and 7.

In contrast, the block GMRES solvers used as a baseline, while effective on ideal Cartesian grids, show significant sensitivity to geometric distortion, especially in three dimensions and for higher-order elements, where they occasionally fail to converge for highly distorted meshes. While they can provide a simpler implementation, their performance gap compared to the Braess–Sarazin approach widens as the difficulty of the problem increases. These results confirm that the tight coupling of velocity and pressure within the Braess–Sarazin smoother is essential for achieving robustness on the distorted or unstructured patches that comprise a general finite element mesh.

### 3.2 Application in Geometric Multigrid

Having established the performance of the local solvers on a single patch, we now return to their application as smoothers within the global geometric multigrid algorithm. In a practical multigrid setting, the local problem on each patch does not need to be solved to high accuracy. The goal of the smoother is to damp high-frequency error components, which can typically be achieved with just a few iterations of an effective iterative method.

We denote by  $N_{\text{MG}}$  the number of local iterations (e.g., p-multigrid V-cycles or Braess–Sarazin steps) applied within each local patch solve. Based on the local solver analysis, we focus on the Braess–Sarazin smoother configured with a single Richardson iteration for the inner Schur complement solve. This configuration offers the best balance of cost and robustness. We compare it against a standard Block-Triangular (Block MG) preconditioner and a direct (exact) solver on each patch.

We evaluate the performance on a 2D test problem. The implementation of the patch smoother in 2D is currently matrix-based and unoptimized compared to the matrix-free 3D implementation, but it allows for rigorous testing of numerical robustness. We start with a coarse grid of  $3 \times 3$  cells. This specific discretization is chosen to allow for a central cell that is isolated from the domain boundary, which we will use to test coefficient jumps. This coarse grid is refined uniformly to generate a hierarchy of meshes (typically  $L = 4$  levels). To assess robustness against grid quality, we introduce random geometric distortions. The interior vertices of the fine grid are perturbed by a random vector of magnitude  $\delta h$ , where  $h$  is the local cell width and  $\delta \in \{0, 10\%, 25\%, 35\%\}$  is the distortion parameter.

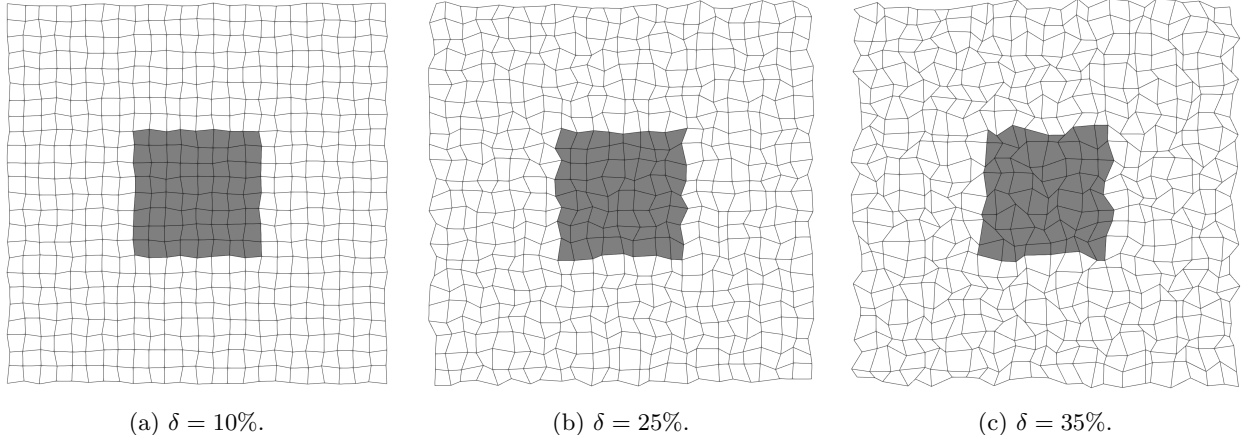


Figure 8: Meshes with  $L = 4$  multigrid levels used in the numerical experiments to assess robustness to geometric distortion. 2D mesh distorted by various factors  $\delta \in \{10\%, 25\%, 35\%\}$ . The shaded region indicates the subdomain of high viscosity used in the coefficient-jump test.

The patch smoother is applied multiplicatively within a global geometric multigrid V-cycle with one pre- and one post-smoothing step. We use FGMRES as the outer solver and iterate until the relative residual is reduced by  $10^{-8}$ .

Interestingly, the global GMRES iteration counts are notably low, often appearing even more favorable than the convergence rates observed for isolated local problems. This effect is a direct consequence of the overlapping structure of the vertex-patch smoother: in a multiplicative sweep over a structured  $d$ -dimensional mesh, each cell is contained within  $2^d$  different patches. As a result, the degrees of freedom on each cell are updated multiple times during a single global smoothing step, significantly enhancing the error damping. A similar observation was made and analyzed for the scalar Laplace problem in [42].

Table 2 presents the results for the stationary Stokes problem with constant coefficients. We observe that the simple Block MG approach is not robust. It fails to converge (NC) for  $N_{\text{MG}} = 1$  and degrades significantly with mesh distortion and increasing polynomial degree  $p$ , even with more local iterations. In sharp contrast, the Braess-Sarazin smoother with just a single step ( $N_{\text{MG}} = 1$ ) delivers excellent performance. Its iteration counts are almost identical to those obtained using an exact local solver, showcasing its ability to effectively handle the saddle-point nature of the equations locally. This robustness holds true even for high polynomial degrees ( $p = 7$ ) and severe mesh distortion ( $\delta = 35\%$ ).

A significant challenge for Stokes solvers is robustness in the presence of large jumps in material coefficients. To test this, we utilize the central cell of our  $3 \times 3$  coarse grid. We assign a viscosity of  $\mu = 10^6$  to this central cell (and all its fine-grid descendants), while the rest of the domain has  $\mu = 1$ .

Table 3 compares the performance of the Braess-Sarazin smoother against the exact local solver in this setting. The results are compelling: the Braess-Sarazin smoother ( $N_{\text{MG}} = 1$ ) maintains iteration counts that are remarkably close to the exact local solve, even with the  $10^6$  jump in viscosity and large mesh distortions. This confirms that the Braess-Sarazin approach correctly captures the local scalings induced by the coefficient jump and separates them from the global smoothing process.

Table 2: GMRES iteration counts (2D, problem with  $L = 4$  multigrid levels) for a geometric multigrid preconditioner using the patch smoother with a local p-multigrid solver. Columns show increasing mesh distortion  $\delta$ . The third column lists  $N_{\text{MG}}$  (number of local p-multigrid cycles) for each row. Entries are FGMRES iteration counts to reduce the residual by  $10^{-8}$ . “NC” indicates no convergence within the iteration limit used in the experiments.

$p$	Local solver	$N_{\text{MG}}$	$\delta = 0\%$	$\delta = 10\%$	$\delta = 25\%$	$\delta = 35\%$
2	Block MG	1	NC	NC	NC	NC
		2	7	7	9	10
	Braess–Sarazin	1	7	7	8	9
	Exact	–	7	7	8	9
3	Block MG	1	NC	NC	NC	NC
		2	7	7	9	12
		3	6	7	8	17
	Braess–Sarazin	1	6	7	8	10
4	Block MG	1	NC	NC	NC	NC
		2	6	7	12	17
		3	6	7	10	NC
	Braess–Sarazin	1	6	7	8	9
7	Block MG	1	NC	NC	NC	NC
		2	12	22	NC	NC
		3	11	NC	NC	NC
	Braess–Sarazin	1	8	8	10	12
		2	6	7	8	9
	Exact	–	5	6	7	8

Table 3: GMRES iteration counts (2D,  $\mu = 10^6$ , with  $L = 4$  multigrid levels) comparing the Braess–Sarazin local smoother with one and two local  $p$ -multigrid cycles and the exact local solve. Columns show increasing mesh distortion  $\delta$ . Entries are FGMRES iteration counts to reduce the residual by  $10^{-8}$ .

$p$	Local solver	$N_{\text{MG}}$	$\delta = 0\%$	$\delta = 10\%$	$\delta = 25\%$	$\delta = 35\%$
2	Braess–Sarazin	1	6	7	9	9
		2	6	7	9	10
	Exact	–	6	7	8	10
3	Braess–Sarazin	1	6	7	8	10
		2	6	7	8	9
	Exact	–	6	7	8	9
4	Braess–Sarazin	1	6	6	8	9
		2	6	6	7	8
	Exact	–	6	6	8	8
7	Braess–Sarazin	1	8	8	10	12
		2	6	6	8	9
	Exact	–	5	6	7	7

## 4 Conclusion

In this work, we investigated the feasibility of using fully iterative, multigrid-based solvers for the local patch problems in Stokes smoothers. Our goal was to determine if an *inexact* solver could maintain global robustness while avoiding the memory and computational costs of direct dense factorizations, which become prohibitive for high-order discretizations.

Among the strategies tested, the Braess–Sarazin smoother emerged as a particularly strong candidate for the local solve. Even when approximating the velocity inverse with a simple  $p$ -multigrid cycle, it demonstrated resilience to mesh distortion and high-contrast viscosity coefficients. These results suggest that maintaining the saddle-point structure within the patch is more beneficial than striving for high precision with decoupled block solvers. Moreover, the efficiency of the Braess–Sarazin approach within the global multigrid hierarchy is striking: a single local application ( $N_{\text{MG}} = 1$ ) yields global iteration counts that are virtually identical to those obtained using an exact direct solver on the patches. In contrast, standard block solvers frequently failed to ensure global convergence under similar conditions, even when allowed multiple local iterations.

It is important to note that while the numerical experiments in this paper were conducted using sparse matrix data structures to facilitate rapid prototyping, the algorithms are designed specifically for a matrix-free context. The iteration counts and robustness observed here serve as a validation for future high-performance implementations relying on sum-factorization. Looking forward, this recursive smoothing strategy appears especially promising for  $H(\text{div})$ -conforming discretizations, such as Raviart–Thomas elements. Since patch smoothers are often theoretically required for these spaces, having a lean, matrix-free local solver could make high-order flux-continuous schemes significantly more attractive for large-scale Stokes and Navier–Stokes simulations.

## Acknowledgments

The generative AI (Gemini, ChatGPT, Claude) was used to assist in drafting and proofreading parts of this manuscript. Any remaining errors are the author's responsibility.

The author warmly thanks his mother, Grażyna, and his brother, Wiktor, for their support. Special thanks to Micro and Konda, the family cats, for their comforting companionship during the writing of this paper.

## References

- [1] D. ARNDT, W. BANGERTH, M. BERGBAUER, B. BLAIS, M. FEHLING, R. GASSMÖLLER, T. HEISTER, L. HELTAI, M. KRONBICHLER, M. MAIER, P. MUNCH, S. SCHEUERMAN, B. TURCKSIN, S. UZUNBAJAKAU, D. WELLS, AND M. WICHROWSKI, *The deal.II library, version 9.7*, preprint, (2025), <https://dealii.org/deal97-preprint.pdf>.
- [2] D. ARNDT, W. BANGERTH, D. DAVYDOV, T. HEISTER, L. HELTAI, M. KRONBICHLER, M. MAIER, J.-P. PELTERET, B. TURCKSIN, AND D. WELLS, *The deal.II finite element library: Design, features, and insights*, Comput. & Math. Appl., 81 (2021), pp. 407–422, <https://doi.org/10.1016/j.camwa.2020.02.022>, <https://arxiv.org/abs/1910.13247>.
- [3] D. N. ARNOLD, R. S. FALK, AND R. WINTHER, *Multigrid in  $H(\text{div})$  and  $H(\text{curl})$* , Numer. Math., 85 (2000), pp. 197–217, <https://doi.org/10.1007/PL00005386>.
- [4] M. BERGBAUER, P. MUNCH, W. A. WALL, AND M. KRONBICHLER, *High-performance matrix-free unfitted finite element operator evaluation*, SIAM Journal on Scientific Computing, 47 (2025), pp. B665–B689.
- [5] D. BORZACCHIELLO, E. LERICHE, B. BLOTTIÈRE, AND J. GUILLET, *Box-relaxation based multigrid solvers for the variable viscosity Stokes problem*, Computers & Fluids, 156 (2017), pp. 515–525.
- [6] D. BRAESS AND R. SARAZIN, *An efficient smoother for the Stokes problem*, Applied Numerical Mathematics, 23 (1997), pp. 3–19.
- [7] J. H. BRAMBLE, *Multigrid Methods*, no. 294 in Pitman research notes in mathematics series, Longman Scientific, 1993.
- [8] P. D. BRUBECK AND P. E. FARRELL, *A scalable and robust vertex-star relaxation for high-order FEM*, SIAM J. Sci. Comput., 44 (2022), pp. A2991–A3017, <https://doi.org/10.1137/21M1444187>.
- [9] C. BURSTEDDE, L. C. WILCOX, AND O. GHATTAS, *p4est: Scalable algorithms for parallel adaptive mesh refinement on forests of octrees*, SIAM J. Sci. Comput., 33 (2011), pp. 1103–1133.
- [10] L. CHEN, *Multigrid methods for saddle point systems using constrained smoothers*, Computers & Mathematics with Applications, 70 (2015), pp. 2854–2866.
- [11] C. CUI, P. GROSSE-BLEY, G. KANSCHAT, AND R. STRZODKA, *An implementation of tensor product patch smoothers on GPUs*, SIAM Journal on Scientific Computing, 47 (2025), pp. B280–B307.

- [12] C. CUI AND G. KANSCHAT, *A multigrid method for cutfem and its implementation on GPU*, arXiv preprint arXiv:2508.11608, (2025).
- [13] C. CUI AND G. KANSCHAT, *Multigrid methods for the Stokes problem on GPU systems*, Computers & Fluids, (2025), p. 106703.
- [14] M. O. DEVILLE, P. F. FISCHER, AND E. H. MUND, *High-order methods for incompressible fluid flow*, vol. 9, Cambridge university press, 2002.
- [15] P. E. FARRELL, Y. HE, AND S. P. MACLACHLAN, *A local Fourier analysis of additive Vanka relaxation for the Stokes equations*, Numerical Linear Algebra with Applications, 28 (2021), p. e2306.
- [16] W. HACKBUSCH, *Multi-grid Methods and Applications*, Springer, Heidelberg, 1985.
- [17] G. HARPER AND R. TUMINARO, *Compression and reduced representation techniques for patch-based relaxation*, arXiv preprint arXiv:2306.10025, (2023).
- [18] Q. HONG, J. KRAUS, J. XU, AND L. ZIKATANOV, *A robust multigrid method for discontinuous Galerkin discretizations of Stokes and linear elasticity equations*, Numer. Math., 132 (2016), pp. 23–49.
- [19] B. JANSSEN AND G. KANSCHAT, *Adaptive multilevel methods with local smoothing for  $H^1$ - and  $H^{\text{curl}}$ -conforming high order finite element methods*, SIAM J. Sci. Comput., 33 (2011), pp. 2095–2114, <https://doi.org/10.1137/090778523>.
- [20] D. JODLBAUER, U. LANGER, T. WICK, AND W. ZULEHNER, *Matrix-free monolithic multigrid methods for Stokes and generalized Stokes problems*, SIAM Journal on Scientific Computing, 46 (2024), pp. A1599–A1627.
- [21] G. KANSCHAT AND Y. MAO, *Multigrid methods for  $\mathbf{H}^{\text{div}}$ -conforming discontinuous Galerkin methods for the Stokes equations*, J. Numer. Math., 23 (2015), pp. 51–66, <https://doi.org/10.1515/jnma-2015-0005>.
- [22] M. KRONBICHLER AND K. KORMANN, *A generic interface for parallel cell-based finite element operator application*, Computers & Fluids, 63 (2012), pp. 135–147, <https://doi.org/10.1016/j.compuid.2012.04.012>.
- [23] M. KRONBICHLER AND K. KORMANN, *Fast matrix-free evaluation of discontinuous Galerkin finite element operators*, ACM Trans. Math. Softw., 45 (2019), pp. 29/1–40, <https://doi.org/10.1145/3325864>.
- [24] M. KRONBICHLER AND K. LJUNGKVIST, *Multigrid for matrix-free high-order finite element computations on graphics processors*, ACM Trans. Parallel Comput., 6 (2019), pp. 2/1–32, <https://doi.org/10.1145/3322813>.
- [25] P. KRZYZANOWSKI, *On block preconditioners for nonsymmetric saddle point problems*, SIAM Journal on Scientific Computing, 23 (2001), pp. 157–169.
- [26] P. KRZYŻANOWSKI, *On block preconditioners for saddle point problems with singular or indefinite (1, 1) block*, Numerical Linear Algebra with Applications, 18 (2011), pp. 123–140.

[27] R. E. LYNCH, J. R. RICE, AND D. H. THOMAS, *Direct solution of partial difference equations by tensor product methods*, Numer. Math., 6 (1964), pp. 185–199, <https://doi.org/10.1007/BF01386067>.

[28] N. MARGENBERG, M. BAUSE, AND P. MUNCH, *An  $hp$  multigrid approach for tensor-product space-time finite element discretizations of the Stokes equations*, arXiv preprint arXiv:2502.09159, (2025).

[29] N. MARGENBERG, M. BAUSE, AND P. MUNCH, *An multigrid approach for tensor-product space-time finite element discretizations of the Stokes equations*, SIAM Journal on Scientific Computing, 47 (2025), pp. B1503–B1529.

[30] D. A. MAY, J. BROWN, AND L. LE POURHIET, *A scalable, matrix-free multigrid preconditioner for finite element discretizations of heterogeneous Stokes flow*, Computer methods in applied mechanics and engineering, 290 (2015), pp. 496–523.

[31] P. MUNCH AND M. KRONBICHLER, *Cache-optimized and low-overhead implementations of additive Schwarz methods for high-order FEM multigrid computations*, Int. J. High Perf. Comput. Appl., (2023), <https://doi.org/10.1177/10943420231217221>. In press.

[32] J.-C. NÉDÉLEC, *Mixed finite elements in  $\mathbb{R}^3$* , Numerische Mathematik, 35 (1980), pp. 315–341, <https://doi.org/10.1007/BF01396415>.

[33] M. A. OLSHANSKII, J. PETERS, AND A. REUSKEN, *Uniform preconditioners for a parameter dependent saddle point problem with application to generalized Stokes interface equations*, Numerische Mathematik, 105 (2006), pp. 159–191.

[34] L. F. PAVARINO, *Additive Schwarz methods for the  $p$ -version finite element method*, Numerische Mathematik, 66 (1993), pp. 493–515.

[35] W. PAZNER, *Efficient low-order refined preconditioners for high-order matrix-free continuous and discontinuous Galerkin methods*, SIAM Journal on Scientific Computing, 42 (2020), pp. A3055–A3083.

[36] P.-A. RAVIART AND J.-M. THOMAS, *A mixed finite element method for 2nd order elliptic problems*, in Mathematical aspects of finite element methods, I. Galligani and E. Magenes, eds., vol. 606, 1977, pp. 292–315, <https://doi.org/10.1007/BFb0064470>.

[37] J. RUDI, G. STADLER, AND O. GHATTAS, *Weighted BFBT preconditioner for Stokes flow problems with highly heterogeneous viscosity*, SIAM Journal on Scientific Computing, 39 (2017), pp. S272–S297.

[38] J. L. THOMAS, B. DISKIN, AND A. BRANDT, *Textbook multigrid efficiency for fluid simulations*, Annu. Rev. Fluid Mech., 35 (2003), pp. 317–340, <https://doi.org/10.1146/annurev.fluid.35.101101.161209>.

[39] S. P. VANKA, *Block-implicit multigrid solution of Navier-Stokes equations in primitive variables*, Journal of Computational Physics, 65 (1986), pp. 138–158.

[40] A. VORONIN, S. MACLACHLAN, L. N. OLSON, AND R. S. TUMINARO, *Monolithic algebraic multigrid preconditioners for the Stokes equations*, SIAM Journal on Scientific Computing, 47 (2025), pp. A343–A373.

- [41] M. WICHROWSKI, *A geometric multigrid preconditioner for discontinuous Galerkin shifted boundary method*, arXiv preprint arXiv:2506.12899, (2025).
- [42] M. WICHROWSKI, *Local solvers for high-order patch smoothers via  $p$ -multigrid*, arXiv preprint arXiv:2510.17785, (2025).
- [43] M. WICHROWSKI, *Multigrid  $p$ -robustness at jacobi speeds: Efficient matrix-free implementation of local  $p$ -multigrid solvers*, arXiv preprint arXiv:2512.02577, (2025).
- [44] M. WICHROWSKI AND P. KRZYŻANOWSKI, *A matrix-free multilevel preconditioner for the generalized Stokes problem with discontinuous viscosity*, Journal of Computational Science, 63 (2022), p. 101804.
- [45] M. WICHROWSKI, P. KRZYŻANOWSKI, L. HELTAI, AND S. STUPKIEWICZ, *Exploiting high-contrast Stokes preconditioners to efficiently solve incompressible fluid–structure interaction problems*, International Journal for Numerical Methods in Engineering, 124 (2023), pp. 5446–5470.
- [46] M. WICHROWSKI, P. MUNCH, M. KRONBICHLER, AND G. KANSCHAT, *Smoothers with localized residual computations for geometric multigrid methods for higher-order finite elements*, SIAM Journal on Scientific Computing, 47 (2025), pp. B645–B664.
- [47] J. WITTE, D. ARNDT, AND G. KANSCHAT, *Fast tensor product Schwarz smoothers for high-order discontinuous Galerkin methods*, Comput. Meth. Appl. Math., 21 (2021), pp. 709–728, <https://doi.org/10.1515/cmam-2020-0078>.
- [48] J. WITTE, C. CUI, F. BONIZZONI, AND G. KANSCHAT, *Tensor-product vertex patch smoothers for biharmonic problems*, Computational Methods in Applied Mathematics, (2025).
- [49] H. WOBKER AND S. TUREK, *Numerical studies of Vanka-type smoothers in computational solid mechanics*, Advances in Applied Mathematics and Mechanics, 1 (2009), pp. 29–55.
- [50] W. ZULEHNER, *A class of smoothers for saddle point problems*, Computing, 65 (2000), pp. 227–246.

## A Closed form of the local inverse approximate and computational complexity estimate

The local solver via the  $p$ -multigrid method employing a Braess–Sarazin smoother on each level yields an approximate inverse of the Stokes operator on a single patch that can be written down explicitly. In this appendix, we derive the closed-form expression for this operator to illustrate that every component can be evaluated solely using Kronecker products of one-dimensional matrices, and also for a bit of mathematical fun.

### A.1 Level and Transfer Operators

Let  $k = 1, \dots, L$  denote the local  $p$ -multigrid levels, corresponding to polynomial degrees  $p_1 < p_2 < \dots < p_L$ . We denote the finite element spaces on level  $k$  as  $\mathbb{V}_k \times \mathbb{Q}_k$ . Note that for the coarsest level  $k = 1$  (corresponding to  $p = 1$ ), the pressure space is effectively empty due to the mean value constraint on a single macro-element, so we perform calculations only on the velocity space  $\mathbb{V}_1$ .

The discrete Stokes operator on level  $k$  is given by

$$\mathcal{A}_k = \begin{pmatrix} A_k & B_k^T \\ B_k & 0 \end{pmatrix}. \quad (8)$$

For  $k = 1$ , this reduces to  $\mathcal{A}_1 = A_1$ .

We define the prolongation operators  $\mathcal{P}_{k-1}^k : (\mathbb{V}_{k-1} \times \mathbb{Q}_{k-1}) \rightarrow (\mathbb{V}_k \times \mathbb{Q}_k)$  as the natural finite element embeddings. We assume that the finite element spaces are constructed as tensor products of one-dimensional spaces. This property is satisfied by common choices such as the  $\mathbb{Q}_p - \mathbb{Q}_{p-2}^{DG}$  pair as well as Raviart–Thomas of degree  $p$  elements and their corresponding pressure spaces  $\mathbb{Q}_p^{DG}$ .

The mentioned operators exhibit a tensor-product structure. Specifically, for a  $d$ -dimensional patch, the transfer operator can be written as a Kronecker product of 1D transfer matrices:

$$P_{k-1}^k = P_{1D} \otimes \dots \otimes P_{1D}, \quad (9)$$

where  $P_{1D} \in \mathbb{R}^{(p_k+1) \times (p_{k-1}+1)}$  is the 1D embedding matrix. The restriction operators  $\mathcal{R}_k^{k-1}$  are the adjoints of the prolongations.

The efficient implementation of the local solver should rely on the fact that both transfer operators and level operators can be evaluated using sum factorization. To define the level operators  $A_k$  and  $B_k$ , let  $V_k, D_k \in \mathbb{R}^{n_q \times (p_k+1)}$  be the 1D Vandermonde (evaluation) and derivative matrices at the quadrature points, and let  $V_{p,k} \in \mathbb{R}^{n_q \times p_k}$  be the corresponding evaluation matrix for the pressure space ( $\mathbb{Q}_{p-1}$ ). In 3D, we define the gradient operators on the reference cell as:

$$\hat{\nabla}_1 = D_k \otimes V_k \otimes V_k, \quad \hat{\nabla}_2 = V_k \otimes D_k \otimes V_k, \quad \hat{\nabla}_3 = V_k \otimes V_k \otimes D_k. \quad (10)$$

Let  $J = \frac{\partial x}{\partial \xi}$  be the mapping Jacobian,  $G = J^{-T}$  be its inverse transpose, and  $W = \text{diag}(w_q) \det(J)$  be the diagonal matrix of quadrature weights scaled by the determinant of the Jacobian.

The physical gradients are then given by  $\nabla_j = \sum_{i=1}^3 G_{ij} \hat{\nabla}_i$ . The velocity block  $A_{k,1}$  (for a single component) and the divergence blocks  $B_{k,j}$  can be expressed as:

$$A_{k,1} = \sum_{j=1}^3 \nabla_j^T W \nabla_j, \quad B_{k,j} = \mathbf{V}_{p,k}^T W \nabla_j, \quad (11)$$

where  $\mathbf{V}_{p,k} = V_{p,k} \otimes V_{p,k} \otimes V_{p,k}$  is the 3D pressure evaluation operator.

Since  $W$  and  $G$  are constant, the evaluation remains a structured sequence of 1D operations. For instance, the action of one reference gradient component on a vector  $u$  is evaluated as:

$$(V_k \otimes V_k \otimes D_k)u = (V_k \otimes I \otimes I)(I \otimes V_k \otimes I)(I \otimes I \otimes D_k)u. \quad (12)$$

This decomposition reduces the computational complexity from  $O((p+1)^6)$  to  $O((p+1)^4)$ , which is crucial for high polynomial degrees. Note that these estimates require the underlying elements to have a tensor-product structure. This includes Raviart–Thomas elements, which, despite their more complex definition, maintain this structure and thus benefit from the same gains in efficiency[13].

## A.2 The Braess–Sarazin Smoother

On each level  $k > 1$ , we apply a smoother  $\mathcal{S}_k$ . The action of the inverse  $\mathcal{S}_k^{-1}$  corresponds to one iteration of the Braess–Sarazin method with approximated Schur complement. Let  $r = (r_u, r_p)^T$  be the residual. The smoothing step  $x_{new} = x_{old} + \mathcal{S}_k^{-1}(r - \mathcal{A}_k x_{old})$  (with initial guess zero for the correction) produces a correction  $(\delta u, \delta p)^T$  computed as follows:

1.  $\delta u^{(1)} = \tilde{A}_k^{-1}r_u,$
2.  $\delta p = \tilde{S}_k^{-1}(B_k \delta u^{(1)} - r_p),$
3.  $\delta u = \delta u^{(1)} - \tilde{A}_k^{-1}B_k^T \delta p.$

Here,  $\tilde{A}_k$  and  $\tilde{S}_k$  are diagonal scaling matrices incorporating relaxation parameters  $\omega_a$  and  $\omega_s$ :

$$\tilde{A}_k^{-1} = \omega_a(\text{diag}(A_k))^{-1}, \quad \tilde{S}_k^{-1} = \omega_s(\text{diag}(S_k))^{-1}, \quad (13)$$

where  $S_k = B_k \tilde{A}_k^{-1} B_k^T$  is the Schur complement associated with the preconditioner  $\tilde{A}_k$ .

We can express the action of  $\mathcal{S}_k^{-1}$  in block matrix form. Substituting step 1 into 2, we get

$$\delta p = \tilde{S}_k^{-1}B_k \tilde{A}_k^{-1}r_u - \tilde{S}_k^{-1}r_p. \quad (14)$$

Then, substituting  $\delta p$  into step 3:

$$\delta u = \tilde{A}_k^{-1}r_u - \tilde{A}_k^{-1}B_k^T(\tilde{S}_k^{-1}B_k \tilde{A}_k^{-1}r_u - \tilde{S}_k^{-1}r_p) \quad (15)$$

$$= (\tilde{A}_k^{-1} - \tilde{A}_k^{-1}B_k^T \tilde{S}_k^{-1}B_k \tilde{A}_k^{-1})r_u + \tilde{A}_k^{-1}B_k^T \tilde{S}_k^{-1}r_p. \quad (16)$$

Thus, the operator  $\mathcal{S}_k^{-1}$  is explicitly given by

$$\mathcal{S}_k^{-1} = \begin{pmatrix} \tilde{A}_k^{-1} - \tilde{A}_k^{-1}B_k^T \tilde{S}_k^{-1}B_k \tilde{A}_k^{-1} & \tilde{A}_k^{-1}B_k^T \tilde{S}_k^{-1} \\ \tilde{S}_k^{-1}B_k \tilde{A}_k^{-1} & -\tilde{S}_k^{-1} \end{pmatrix}. \quad (17)$$

## A.3 The p-Multigrid Operator

Let  $\mathcal{M}_k^{-1}$  denote the approximate inverse of  $\mathcal{A}_k$  provided by the  $p$ -multigrid V-cycle with one pre-smoothing and one post-smoothing step per level.

On the coarsest level  $k = 1$ , the problem is solved exactly for the velocity:

$$\mathcal{M}_1^{-1} = A_1^{-1}. \quad (18)$$

Note that  $A_1$  is a  $3 \times 3$  matrix in 3D and  $2 \times 2$  matrix in 2D, corresponding to the velocity space spanned on a single node.

For  $k > 1$ , the V-cycle operator is defined recursively. The inverse approximate consists of pre-smoothing, followed by the coarse grid correction, and finally post-smoothing:

$$\mathcal{M}_k^{-1} = (2I - \mathcal{S}_k^{-1} \mathcal{A}_k) \mathcal{S}_k^{-1} + (I - \mathcal{S}_k^{-1} \mathcal{A}_k) \mathcal{P}_{k-1}^k \mathcal{M}_{k-1}^{-1} \mathcal{R}_k^{k-1} (I - \mathcal{A}_k \mathcal{S}_k^{-1}). \quad (19)$$

For polynomial degrees  $k = 2, 3$  the above formula does not require any further recursion since the coarsest level  $k = 1$  is reached, where the exact inverse is applied. Hence, we have obtained a closed-form expression for  $\mathcal{M}_k^{-1}$  for those cases, while for higher polynomial degrees the recursion should be expanded further.

#### A.4 Complexity Analysis

The computational complexity of the  $p$ -multigrid cycle is characterized by the number of applications of the discrete velocity Laplacian  $\mathcal{A}_k$  and the divergence operator  $\mathcal{B}_k$  (and its adjoint  $\mathcal{B}_k^T$ ) on the finest level. We assume that applying the diagonal inverse of  $\mathcal{A}_k$  (and similarly for the Schur complement) is negligible compared to the cost of the matrix-vector multiplications. Consequently, we quantify the complexity by the total number  $N_A$  and  $N_B$  of applications of  $\mathcal{A}_k$  and  $\mathcal{B}_k$ , respectively. We further assume that the cost of applying  $\mathcal{B}_k$  and  $\mathcal{B}_k^T$  is the same.

When a single Richardson iteration ( $n_S = 1$ ) is used for the inner Schur complement solve, the application of  $\mathcal{S}_k^{-1}$  involves exactly one multiplication by  $\mathcal{B}_k$  to form the pressure right-hand side and one by  $\mathcal{B}_k^T$  to update the velocity correction. Thus, one full smoothing step consisting of an operator application  $\mathcal{A}_k$  followed by the application of  $\mathcal{S}_k^{-1}$  requires  $1\mathcal{A}_k$ ,  $2\mathcal{B}_k$ , and  $2\mathcal{B}_k^T$ .

Consider a V-cycle with  $m$  pre-smoothing and  $m$  post-smoothing steps. In addition to the  $2m$  smoothing steps, the multigrid cycle requires one additional application of  $\mathcal{A}_k$  to compute the defect for the restriction to the coarser levels. The total number of multiplications on the finest level is:

$$N_A = 2m + 1, \quad N_B = 2m + (2m + 1) = 4m + 1. \quad (20)$$

For the standard configuration used throughout this work ( $m = 1$ ,  $n_S = 1$ ), the cost on the finest level is exactly  $N_A = 3$  and  $N_B = 5$ .

We also express the cost in terms of sum-factorization kernels, where each kernel represents the application of a  $d$ -dimensional tensor-product operator (e.g.,  $X \otimes Y \otimes Z$  in 3D). For a stationary Stokes problem, evaluation of  $\mathcal{A}_k$  requires 18 sum-factorization kernels (9 gradient components times 2 for the application and its transpose), while evaluation of  $\mathcal{B}_k$  requires 10 sum-factorization kernels (9 gradient components to compute divergence and one to multiply by pressure and integrate). This results in the cost of operator  $\mathcal{A}_k$  being 38 sum-factorization kernels while the cost of all smoothing steps (one pre- and one post-smoothing step) is 116 sum-factorization kernels. The cost of transfer operators requires an additional 6 sum-factorization kernels (3 for prolongation and 3 for restriction) while the cost of evaluation on the coarser levels operators is less than  $1/4$  of the cost of the finest level. Thus, the total cost of the  $p$ -multigrid V-cycle with one pre- and one post-smoothing step cost approximately the same as 152 sum-factorization kernels on the finest level, that is around 4.0 times the cost of a single application of the discrete Stokes operator  $\mathcal{A}_k$ . In [43], empirical measurements for the Poisson equation showed a cost of approximately 2.27 times the operator application.

Note that mileage may vary: on modern architectures some operations are cheaper than others so the cost will be hardware dependent. Additionally, in the application of  $\mathcal{A}_k$  some operations may be fused, or lower precision computations may be used in  $p$ -multigrid cycle to reduce the effective cost, so this is a rough estimate. Finally, on Cartesian grids some optimizations are possible.